NOTES AND CORRESPONDENCE

Interdecadal Changes of 30-Yr SST Normals during 1871–2000

YAN XUE

NOAA/NWS/NCEP Climate Prediction Center, Camp Springs, Maryland

THOMAS M. SMITH AND RICHARD W. REYNOLDS

NOAA/NESDIS National Climatic Data Center, Asheville, North Carolina

18 March 2002 and 22 November 2002

ABSTRACT

SST predictions are usually issued in terms of anomalies and standardized anomalies relative to a 30-yr normal: climatological mean (CM) and standard deviation (SD). The World Meteorological Organization (WMO) suggests updating the 30-yr normal every 10 yr. In complying with the WMO's suggestion, a new 30-yr normal for the 1971–2000 base period is constructed. To put the new 30-yr normal in historical perspective, all the 30-yr normals since 1871 are investigated, starting from the beginning of each decade (1871–1900, 1881–1910, . . . , 1971–2000). Using the extended reconstructed sea surface temperature (ERSST) on a 2° grid for 1854–2000 and the Hadley Centre Sea Ice and SST dataset (HadISST) on a 1° grid for 1870–1999, eleven 30-yr normals are calculated, and the interdecadal changes of seasonal CM, seasonal SD, and seasonal persistence (*P*) are discussed. The interdecadal changes of seasonal CM are prominent (0.3°–0.6°) in the tropical Indian Ocean, the midlatitude North Pacific, the midlatitude North Atlantic, most of the South Atlantic, and the sub-Antarctic front. Four SST indices are used to represent the key regions of the interdecadal changes: the Indian Ocean (''INDIAN''; 10°S–25°N, 45°–100°E), the Pacific decadal oscillation (PDO; 35°–45°N, 160°E–160°W), the North Atlantic Oscillation (NAO; 40°–60°N, 20°–60°W), and the South Atlantic (SATL; 22°S–2°N, 35°W–10°E). Both INDIAN and SATL show a warming trend that is consistent between ERSST and HadISST. Both PDO and NAO show a multidecadal oscillation that is consistent between ERSST and HadISST except that HadISST is biased toward warm in summer and cold in winter relative to ERSST. The interdecadal changes in Niño-3 (5°S–5°N, 90°–150°W) are small (0.2°) and are inconsistent between ERSST and HadISST. The seasonal SD is prominent in the eastern equatorial Pacific, the North Pacific, and North Atlantic. The seasonal SD in Niño-3 varies interdecadally: intermediate during 1885–1910, small during 1910–65, and large during 1965–2000. These interdecadal changes of ENSO variance are further verified by the Darwin sea level pressure. The seasonality of ENSO variance (smallest in spring and largest in winter) also varies interdecadally: moderate during 1885–1910, weak during 1910–65, and strong during 1965–2000. The interdecadal changes of the seasonal SD of other indices are weak and cannot be determined well by the datasets. The seasonal *P*, measured by the autocorrelation of seasonal anomalies at a two-season lag, is largest in the eastern equatorial Pacific, the tropical Indian, and the tropical North and South Atlantic Oceans. It is also seasonally dependent. The ''spring barrier'' of *P* in Niño-3 (largest in summer and smallest in winter) varies interdecadally: relatively weak during 1885–1910, moderate during 1910–55, strong during 1955–75, and moderate during 1975–2000. The interdecadal changes of SD and *P* not only have important implications for SST forecasts but also have significant scientific values to be explored.

1. Introduction

At the National Oceanic and Atmospheric Administration Climate Prediction Center (CPC), the official forecast for the tropical Pacific sea surface temperature (SST) index is issued as anomalies and standardized anomalies relative to a 30-yr normal: climatological mean (CM) and standard deviation (SD). The World Meteorological Organization (WMO) suggests that the 30-yr normal be based on a 30-yr base period that starts at the beginning of each decade (1951–80, 1961–90, etc.). Although the WMO did not specify the periods on which SD is based, the same base periods are used at CPC for both CM and SD. For a historical reason, the CM originally used at CPC is that calculated for the 1950–79 base period (Reynolds and Smith 1995). To comply with the WMO's standards, the 1961–90 base period was introduced at CPC around 1997 (Smith and Reynolds 1998). In early 2001, CPC was requested to implement the 1971–2000 normal for opera-

Corresponding author address: Dr. Yan Xue, Climate Prediction Center, NCEP/NWS/NOAA, Rm. 605-A, WWB, 5200 Auth Rd., Camp Springs, MD 20746.
E-mail: yan.xue@noaa.gov

tional forecasts. So, we constructed a new SST normal for the 1971–2000 base period and implemented it operationally at CPC in August of 2001 (details were available at the time of writing online at http://www.cpc.ncep.noaa.gov/products/predictions/30day/SSTs/sst_clim.html).

Considering the frequent changes of SST normals used at CPC, we feel that it is useful to compare the new 30-yr normal with previous ones, which include all the 30-yr normals since 1871 (1871–1900, 1881–1910, etc.). The purpose is to show how the 30-yr normals have changed in the past 130 yr and also to provide justification as to why the 30-yr normals need to be updated every 10 yr.

To study the interdecadal changes of 30-yr normals since 1871, we need a long SST dataset. One option is to use the extended reconstructed sea surface temperature (ERSST) by Smith and Reynolds (2003) on a 2° grid for 1854–2000. This analysis is an outgrowth of Smith et al. (1996). The Smith et al. (1996) reconstructed SST overcame the problem of uneven sampling and noisy data by separately analyzing low- and high-frequency variations. The low-frequency variations are analyzed using simple averaging and smoothing, and the high-frequency variations are analyzed by fitting observed high-frequency SST anomalies to a set of empirical orthogonal functions (EOFs). In ERSST, improvements include additional data, an improved data quality control, and an improved statistical analysis method.

A second option is to use the Hadley Centre Sea Ice and Sea Surface Temperature dataset (HadISST) by Rayner et al. (2003, hereinafter RAY) on a 1° grid for 1871–1999. The HadISST data set improves upon the previous Global Sea Ice and Sea Surface Temperature (GISST) dataset and is a unique combination of monthly globally complete fields of SST and sea-ice concentration. Ice-zone SSTs are estimated using statistical relationships between SST and sea-ice concentration. In HadISST, broadscale fields of SST are reconstructed using an EOF-based technique, the reduced-space optimal interpolation described by Kaplan et al. (1998). Smith and Reynolds (2003) did a brief intercomparison of the two datasets and concluded that the large-scale variations of ERSST and HadISST are broadly consistent despite different historical bias corrections and different data and analysis procedures. In this study, the two datasets are used in parallel in computing the 30-yr SST normals since 1871. Our conclusions are based on the consistent results between ERSST and HadISST.

It has been suggested that the interannual variability associated with ENSO is high during 1880–1920 and 1960–90 and low during 1920–60 (Torrence and Compo 1998; Kestin et al. 1998; Mestas-Nuñez and Enfield 2001). Smith (2000) constructed a sea level analysis for the Pacific basin for 1948–98 and found that the variance of monthly sea level anomalies is higher in the second half of the analysis period than that in the first half. Also low-frequency variability not associated with ENSO is found in various ocean basins and seems to have important impacts on regional climates (Allan 2000; Enfield and Mestas-Nuñez 2000). The low-frequency variabilities are often categorized as interdecadal and multidecadal modes and secular trend. By calculating the CM and SD over sliding 30-yr windows in the past 130 yr, we are able to quantify both low- and high-frequency variability. Thus, our analysis not only addresses the interdecadal changes of high-frequency variability associated with ENSO but also those of low-frequency variability not associated with ENSO. In addition to studying CM and SD, we also study the persistence (P) in each 30-yr base period, which is an important quantity in evaluating model forecast skill. In section 2 we describe how the 30-yr SST normals are calculated. In section 3, the interdecadal changes of the CMs of ERSST and HadISST are compared and their consistent features are discussed. Section 4 describes the interdecadal changes of SD and P and their implications for ENSO forecasting. Conclusions and discussion are given in section 5.

2. Data and methods

Because ERSST is on a 2° grid and HadISST is on a 1° grid, we first average HadISST onto a 2° grid. Although the nominal resolution for HadISST is 1° as stated, its real resolution is near 2° after 1949 and near 4° before 1949 (RAY). We compared HadISST with ERSST on both 2° and 4° grids and found that the results are not sensitive to grid resolutions. The results shown below are based on data on a 2° grid unless specifically stated otherwise.

Using ERSST and HadISST, we calculate the 30-yr SST normals for the base periods that start at the beginning of each decade (such as 1871–1900, 1881–1910, . . . , 1971–2000). Because we do not have the HadISST analysis for 2000, the 1971–2000 normal is approximated by the 1971–99 normal. We discuss the seasonal CM and SD only, because the monthly CM and SD convey similar information on the interdecadal changes of 30-yr normals.

To derive the seasonal CM, we first derive the monthly CM by averaging the monthly SST over the appropriate 30-yr base periods. The monthly CM is further smoothed by retaining only the annual mean and first two harmonics. The seasonal CM is calculated by averaging the monthly CM over the appropriate seasons.

To derive the seasonal SD, we first derive monthly anomalies by subtracting the monthly CM from the monthly data, and then we derive seasonal anomalies by averaging the monthly anomalies over the appropriate seasons. The seasonal SD is calculated with seasonal anomalies over the appropriate 30-yr base periods.

In addition to CM and SD, we also calculate the seasonal P in each 30-yr base period, which is measured by the autocorrelation of seasonal anomalies at a two-season lag. For example, the seasonal P in December–

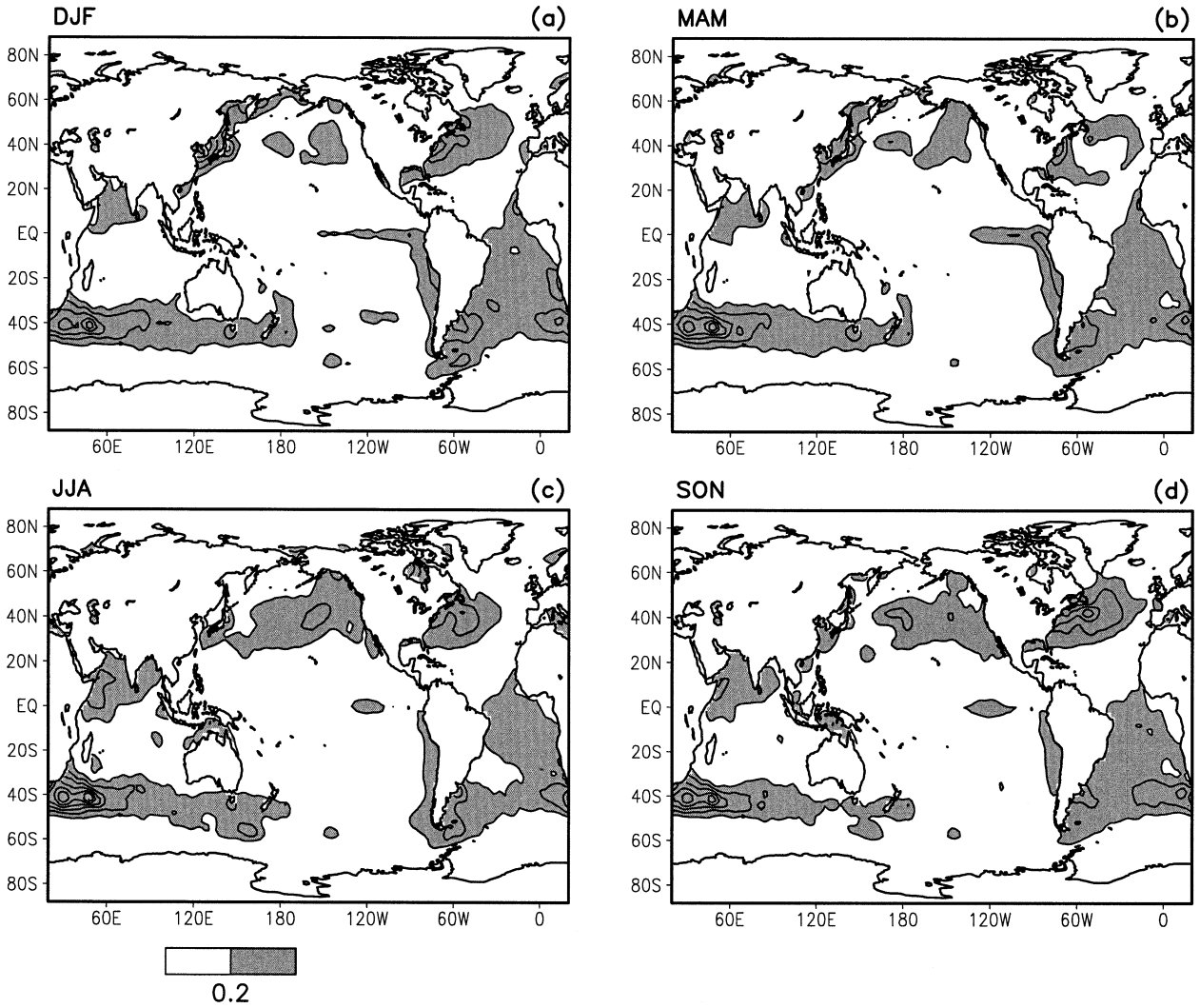

FIG. 1. Standard deviation of the seasonal CM over all the 30-yr base periods during 1871–2000 in the (a) DJF, (b) MAM, (c) JJA, and (d) September–October–November (SON) seasons. The contour interval is 0.1°C. Values less than 0.2° are omitted and greater than 0.2° are shaded.

January–February (DJF) is the autocorrelation between the seasonal anomalies in DJF and the following June–July–August (JJA).

3. Interdecadal changes of climatological mean

The standard deviation of the seasonal CM for the eleven 30-yr base periods, shown in Fig. 1, describes how much the seasonal CM varies over the past 130 yr. Figure 1 shows that the seasonal CM has the largest variations (>0.2) in the tropical Indian Ocean, the midlatitude North Pacific, the midlatitude North Atlantic, most of the South Atlantic, and the sub-Antarctic front in the Atlantic and Indian. The standard deviation of the seasonal CM of HadISST is very similar to that of ERSST but is noisier (not shown). In HadISST, there is a large variation of CM in the Arctic Ocean in summer and in the Pacific-basin portion of the Antarctic Circumpolar Current, which are both absent in ERSST. This is because ERSST does not have sea-ice data.

We use four SST indices to represent the key regions of the largest variations of CM: the Indian Ocean (INDIAN; 10°S–25°N, 45°–100°E), the Pacific decadal oscillation (PDO; 35°–45°N, 160°E–160°W), the North Atlantic Oscillation (NAO; 40°–60°N, 20°–60°W), and the South Atlantic (SATL; 22°S–2°N, 10°E–35°W). The INDIAN index was used by Klein et al. (1999) in studying the Indian Ocean SST response to ENSO, and the PDO index is based on the mode related to the Pacific decadal oscillation (Mantua et al. 1997). The NAO index is based on the air–sea interaction mode related to the North Atlantic Oscillation (Kushnir 1994), and the SATL index was used by Enfield and Mestas-Nuñez (2000) in studying the climate impacts of the South Atlantic SST.

Figure 2a shows the departures of the seasonal CM

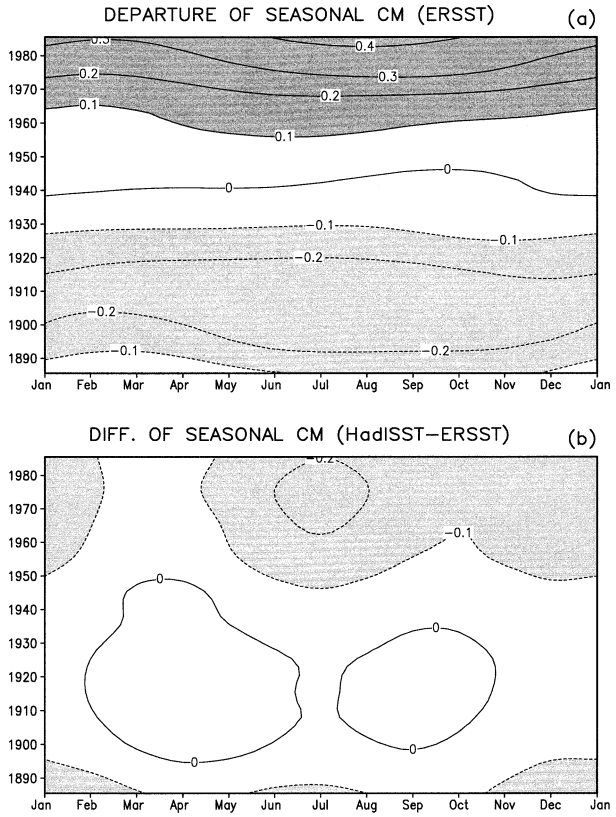

FIG. 2. (a) Departure from the seasonal CM of the INDIAN index (10°S–25°N, 45°–100°E) for ERSST averaged over all the 30-yr base periods during 1871–2000. (b) Differences of the seasonal CM of HadISST and ERSST. The years on the *y* axis are at the centers of the 30-yr base periods, and the months on the *x* axis are at the centers of the seasons. The contour interval is 0.1°C. Values less than −0.1° and greater than 0.1° are shaded.

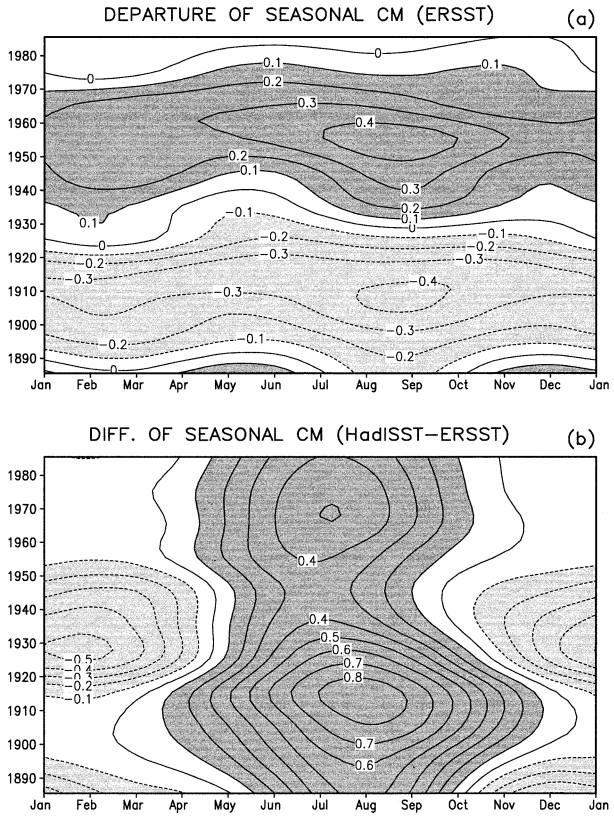

FIG. 3. Same as Fig. 2 but for the PDO index (35°–45°N, 160°E–160°W).

of INDIAN in each 30-yr base period from its average over all 30-yr base periods. It is seen that the tropical Indian Ocean SST as a whole has a warming trend (Bottomley et al. 1990). The change over the past 130 yr is as large as 0.6°. The differences between the seasonal CM of HadISST and ERSST (Fig. 2b) show that HadISST is somewhat cooler than ERSST since 1950, which makes the trend in HadISST slightly less than that in ERSST.

Figure 3a shows that the seasonal CM of PDO has a multidecadal oscillation, relatively warm before 1885, cold during 1890–1930, warm during 1930–75, and cold during 1975–2000. This multidecadal oscillation of PDO is consistent with that discussed by Mantua et al. (1997). However, there is an uncertainty in the result because HadISST is biased toward warm in summer and cold in winter relative to ERSST (Fig. 3b). This bias is as large as 0.8° in summer, which is probably too large to be accounted for by sampling errors given the dense sampling there. For the more limited 1982–99 period, Reynolds et al. (2002, see their Fig. 11) found that the HadISST analysis showed a similar seasonal difference relative to the blended analysis presented there. They suggested that the difference was probably due to different data screening procedures and should be examined in the near future.

An index called the ''interdecadal Pacific oscillation'' (IPO) was recently proposed to represent a Pacific basinwide feature that includes low-frequency variations in climate over both the North and South Pacific (Folland et al. 1999). The time series of this feature is broadly similar to the interdecadal part of the North Pacific PDO index of Mantua et al. (1997). The IPO index of Folland et al. (1999) is characterized using the time series of the third EOF (EOF3) of the 13.3-yr low-pass-filtered global SST for 1911–95. We conducted an EOF analysis similar to that of Folland et al. (1999) using low-pass-filtered seasonal anomalies of ERSST and HadISST on a 4° grid relative to their 1961–90 climatological values in the domain 30°S–60°N. The first three EOFs of ERSST are clearly separable from each other using the criterion of North et al. (1982). Here the degree of freedom was taken to be the number of years in the time series divided by 17 yr. The first EOF (EOF1), accounting for 57% of the total seasonal variance, represents global century-scale trends (Fig. 4). In fact, EOF1 is very similar to the corresponding field of linear SST trends for 1911–95 (not shown). A noticeable difference

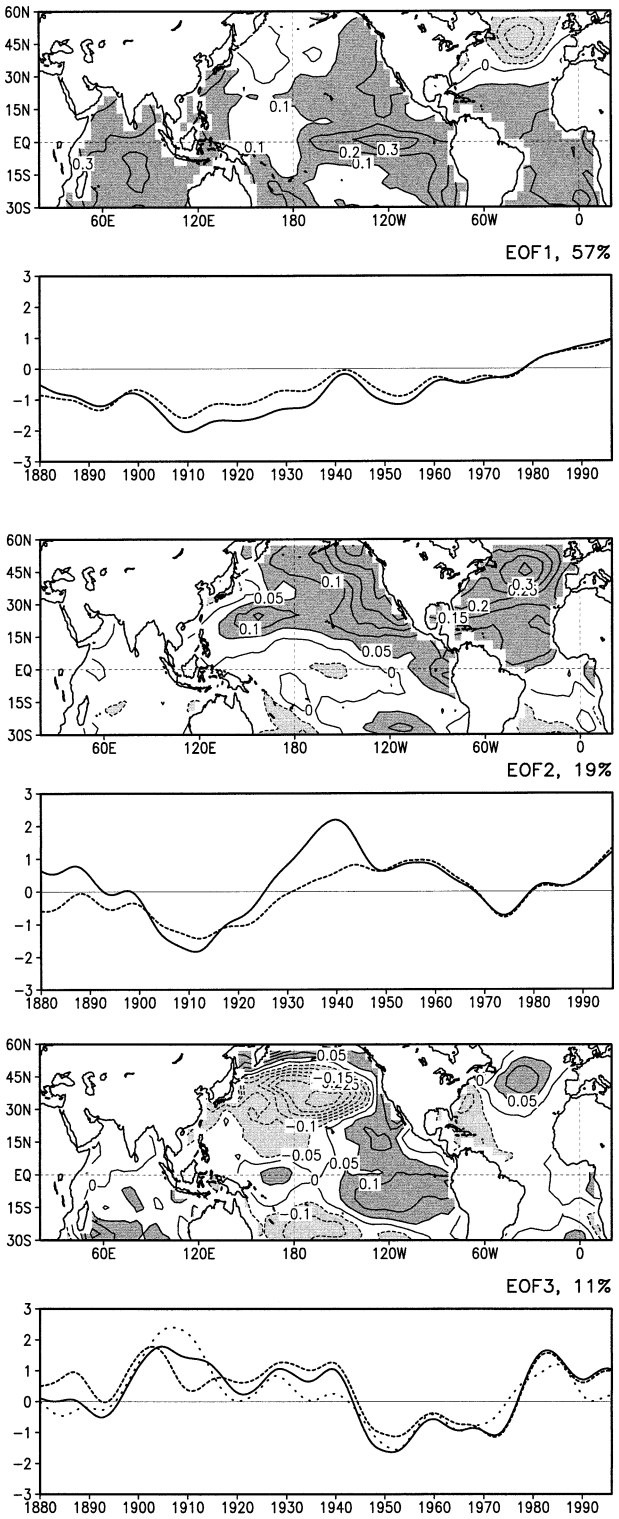

FIG. 4. The first three EOFs of the 13.3-yr low-pass-filtered ERSST for 1911–95. The time series are from projecting the ERSST data onto the eigenvectors (solid line) and from projecting the HadISST data (dashed line). The percent of ERSST variance explained by each mode is indicated. The time series of the PDO index derived from the 13.3-yr low-pass-filtered ERSST is also shown (dotted line) along with the time series of EOF3.

between our EOF1 and that of Folland et al. (1999) is the lack of warming trends along the coastal regions of east Asia. However, the EOF1 of HadISST agrees very well with that of Folland et al. (1999) in those regions (not shown). This result is probably due to the fact that HadISST and the data of Folland et al. (1999) include sea-ice data and ERSST does not. The second EOF (EOF2), accounting for 19% of the total variance, represents the interhemispheric contrast associated with decadal episodes of Sahel wetness or drought (Folland et al. 1999). The time series of projections of ERSST and HadISST onto the EOF2 of ERSST agree well with each other except in 1930–40 and before 1900. EOF3, accounting for 11% of the total variance, is similar to the PDO of Mantua et al. (1997) and particularly to the first global EOF of unfiltered SST of Zhang et al. (1997). The time series of projections of ERSST and HadISST onto the EOF3 of ERSST agree very well with each other except during 1905–15 and before 1890. A PDO index is derived from the 13.3-yr low-pass-filtered data and is compared with the time series of projections of ERSST onto EOF3 (IPO index) in Fig. 4. The IPO index suggests more dramatic climatic transitions around 1944 and 1976 than the PDO index does. Another characteristic of the IPO index is that it strongly influences the relationship between year-to-year Australian climate variations and ENSO and, consequently, the performance of ENSO-based statistical rainfall prediction schemes (Power et al. 1999).

The NAO index also has a multidecadal oscillation, relatively warm before 1890, cold during 1890–1920, warm during 1920–55, and cold during 1955–2000 (Fig. 5a). This multidecadal oscillation of the NAO index is consistent with that discussed by Kushnir (1994). There is a bias between HadISST and ERSST, and the bias is similar to that of PDO but with a smaller amplitude (Figs. 3b and 5b).

Like the INDIAN index, the SATL index has a warming trend (not shown). Because HadISST is biased toward warm relative to ERSST during 1890–1930, the trend in HadISST is slightly less than that in ERSST (not shown).

Because the Niño-3 (5°S–5°N, 90°–150°W) index is widely used in ENSO monitoring and forecasting, it is interesting to know its interdecadal changes. Figure 6a shows that Niño-3 has a warming trend. However, this trend is questionable because HadISST is biased toward warm relative to ERSST during 1890–1950, which overwhelms the trend (Fig. 6b).

The interdecadal changes of SST were explored with surface temperature trend maps in the International Panel on Climate Change (IPCC) science report (Houghton et al. 2001, chapter 2). Using ERSST and HadISST, we computed sea surface temperature trend maps for the 1910–45, 1946–75, and 1976–99 periods similar to those used in the IPCC report. Our trend maps are consistent with those of IPCC except additional information is provided over the missing-value regions in the IPCC

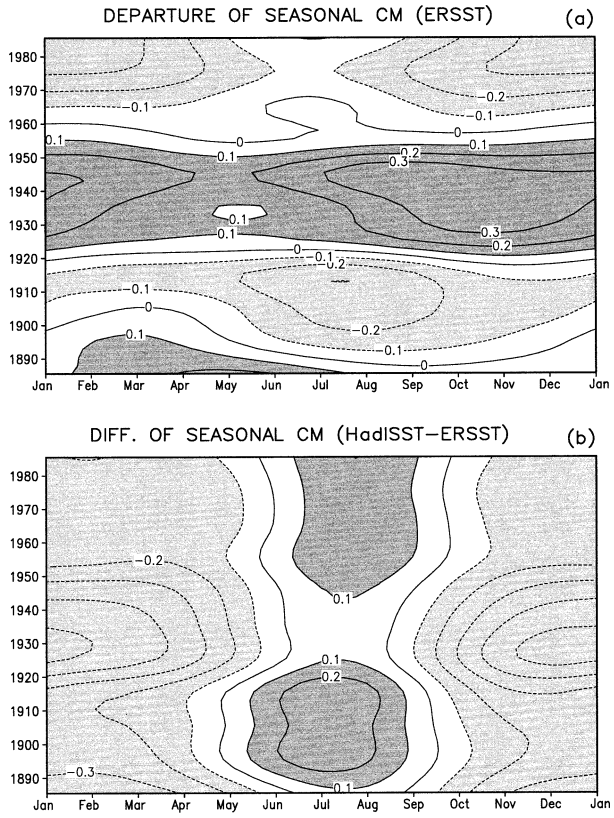

FIG. 5. Same as Fig. 2 but for the NAO index (40°–60°N, 60°–20°W).

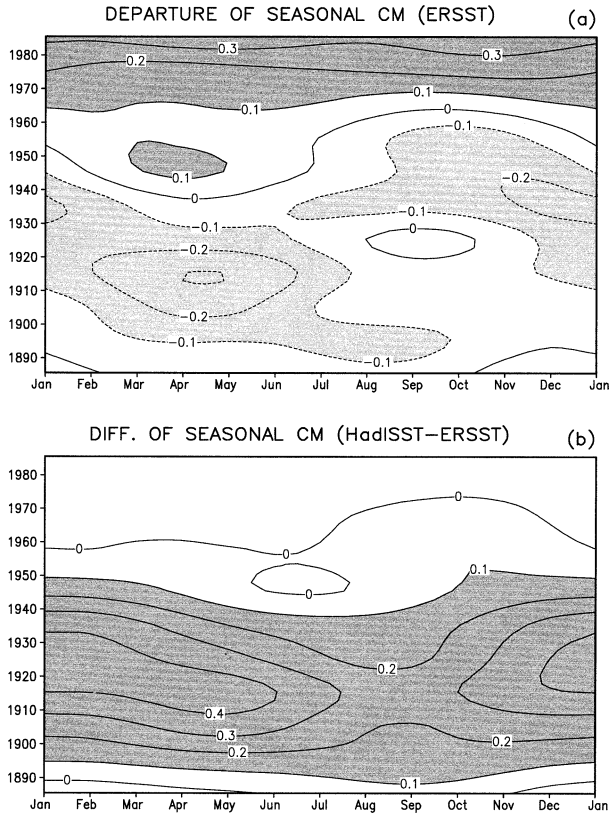

FIG. 6. Same as Fig. 2 but for the Niño-3 index (5°S–5°N, 90°–150°W).

maps. Our trend maps suggest that the warming trend during 1910–45 is not only evident in the Northern Hemisphere but also in the Southern Hemisphere (see Fig. 2.9b of Houghton et al. 2001).

4. Interdecadal changes of standard deviation and persistence

The seasonal SD averaged over the eleven 30-yr base periods, shown in Fig. 7, describes the average seasonal SD in the past 130 yr. It shows that the most prominent interannual variability is in the eastern equatorial Pacific, the North Pacific, the North Atlantic, and some coastal upwelling regions. It is seen that the seasonal SD of HadISST is generally smaller than that of ERSST, especially where the seasonal SD is large. We also compared the seasonal SD of ERSST and HadISST on a 4° grid for 1871–1948; the above results are unchanged. This result suggests that ERSST retains more interannual variance than HadISST does. We think ERSST resolves climate signals better and contains less noise by projecting noisy data onto a set of EOFs. HadISST draws more closely to the noisy data, however, and is more sensitive to sampling than ERSST is (Smith and Reynolds 2003).

Several studies suggest that the interannual variability associated with ENSO varies interdecadally (Torrence and Compo 1998; Kestin et al. 1998). These interdecadal changes of ENSO variance are clearly seen in Fig. 8 where the seasonal SD of Niño-3 in the past 130 yr is shown. The SD of Niño-3 in the last three 30-yr base periods (1951–80, 1961–90, and 1971–2000) shows an upward trend (Fig. 8a). The SD of Niño-3 is intermediate during 1885–1920, small during 1930–50, and large during 1960–2000 (Fig. 8b). The seasonality of SD (smallest in boreal spring and largest in boreal winter) can be monitored by the differences between the winter SD [averaged SD during the November–December–January (NDJ) seasons] and the spring SD [averaged SD during the March–April–May (MAM) seasons]. The spring SD varies from 0.6 to 0.8 and has a dramatic increase since 1965, whereas the winter SD varies from 0.9 to 1.3 and has an upward trend since 1950 (Fig. 8c). The seasonality of SD, measured by the differences between the winter and spring SD, is moderate during 1885–1920, weak during 1930–50, and strong during 1960–2000.

The interdecadal changes of ENSO variance described above are also found in HadISST. However, it is not clear whether the above results are sensitive to sampling changes in the past 130 yr. It can be argued that the recent upward trend of variance might be in-

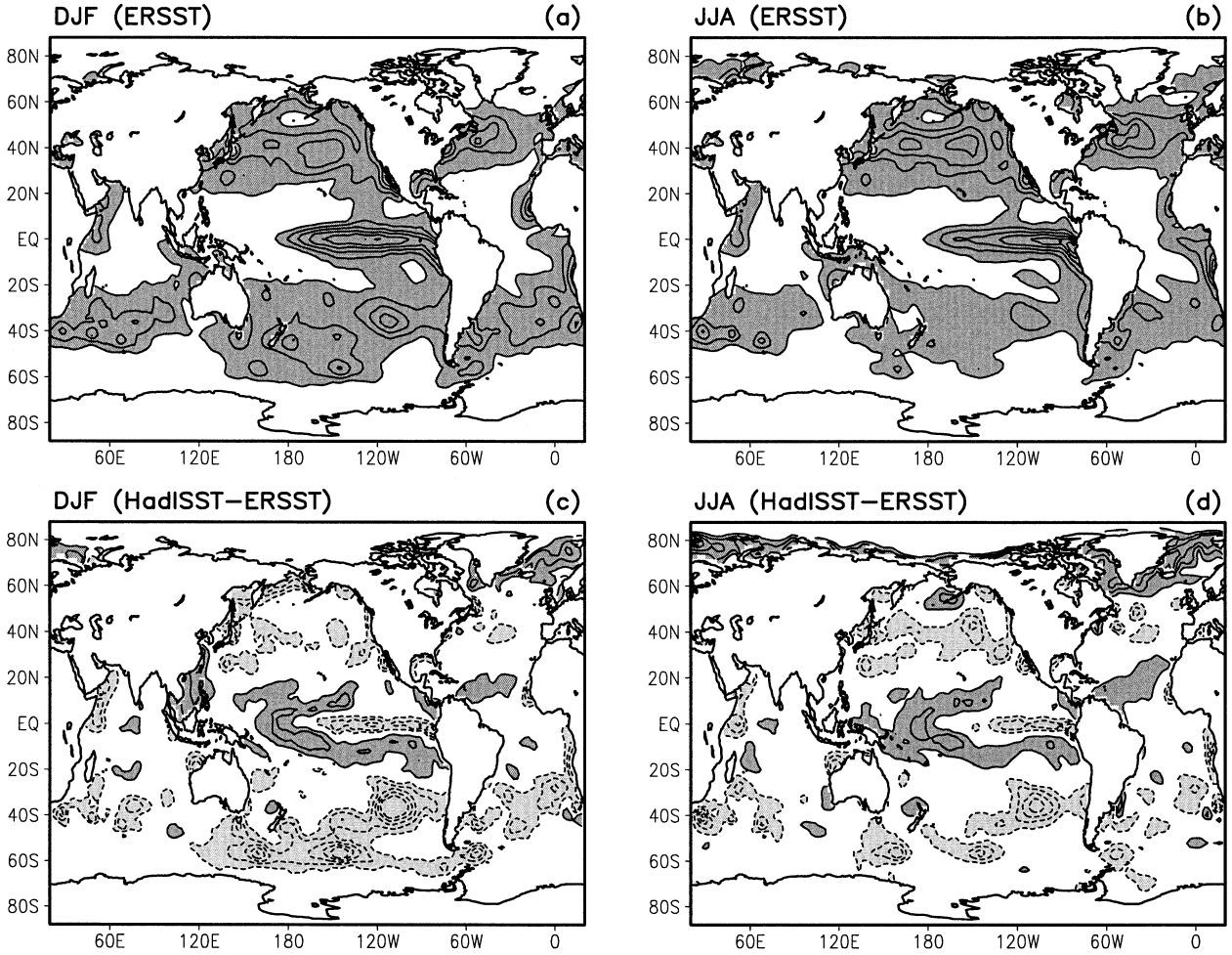

FIG. 7. The seasonal SD of ERSST averaged over all the 30-yr base periods during 1871–2000 in the (a) DJF and (b) JJA seasons. The differences between the seasonal SD of HadISST and ERSST averaged over all the 30-yr base periods during 1871–2000 in (c) the DJF and (d) the JJA seasons. In (a) and (b), the contour interval is 0.2°C, contours less than 0.3° are omitted, and values greater than 0.3° are shaded. In (c) and (d), the contour interval is 0.1°C, and the zero contour is omitted. Values less than −0.1° and greater than 0.1° are shaded.

fluenced by the increase in number of observations, especially from the addition of satellite data beginning in 1981. To check this possibility, we studied the seasonal SD of the Darwin sea level pressure, which has a reliable instrumental record since 1876. The data were downloaded from the Web site of the Australian Bureau of Meteorology (http://www.bom.gov.au/climate/current) and are based on the study by Allan et al. (1991). It is seen in Fig. 9 that the interdecadal changes of ENSO variance described above are also found here. Thus, we conclude that ENSO variance has undergone significant interdecadal changes in the past 130 yr.

We also examined the interdecadal changes of the seasonal SD of PDO and NAO indices. The seasonal SD of PDO averaged over eleven 30-yr base periods shows a seasonality: largest (0.85°C) in summer and smallest (0.65°C) in winter and spring. The interdecadal changes of the seasonal SD of PDO of ERSST is weak (0.1°C). However, in HadISST, the seasonal SD has an upward trend in the past 130 yr with an amplitude of 0.2°–0.3°C (not shown), and its average seasonal SD is 0.7°C in summer and 0.55°C in winter and spring. Because of the inconsistencies between the results of ERSST and HadISST, we conclude that the seasonal SD of PDO and its interdecadal changes may not be well resolved by one or both of the analyses.

The seasonal SD of the NAO index averaged over eleven 30-yr base periods also shows a seasonality: largest (0.65°C) in summer and smallest (0.52°C) in winter and spring. The seasonal SD of NAO of ERSST has a downward trend in the past 130 yr (not shown). In contrast, in HadISST, the seasonal SD of NAO has an upward trend, and the average seasonal SD is 0.62°C in summer and 0.47°C in winter and spring. So, the seasonal SD of NAO and its interdecadal changes may also not be well resolved by one or both of the analyses. We

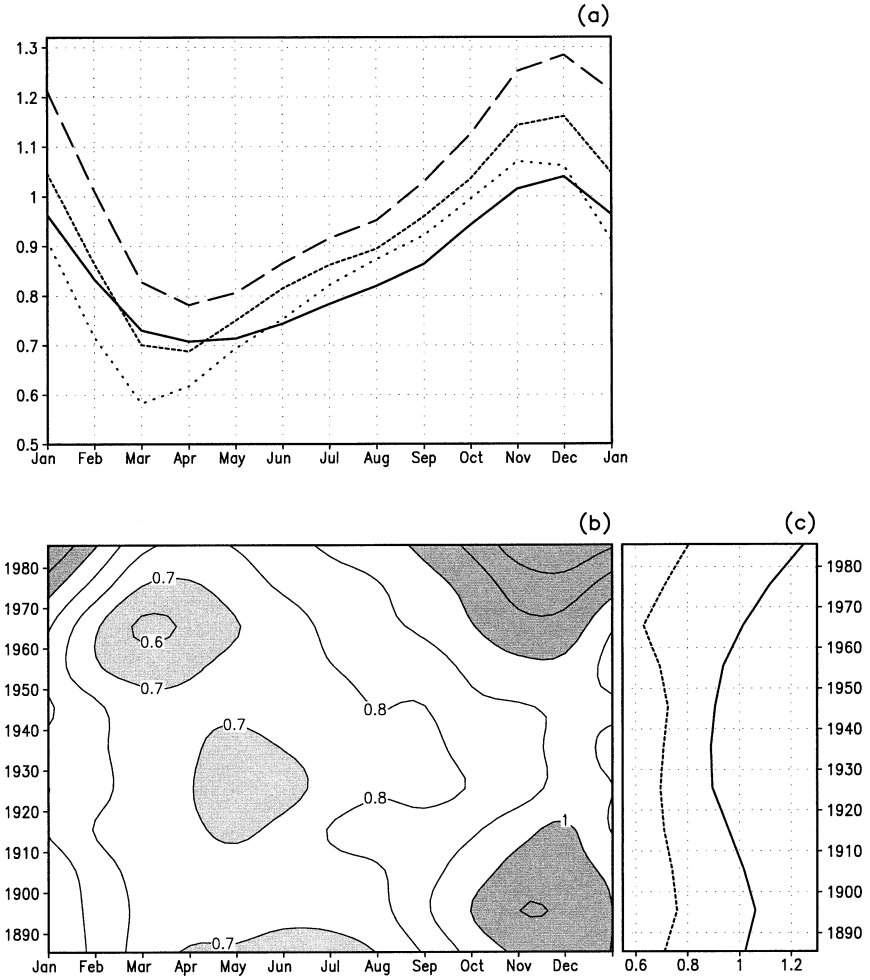

FIG. 8. (a) Annual cycle of the seasonal SD of Niño-3 for the 1971–2000 (long dash), the 1961–90 (short dash), and the 1951–80 (dot) base periods. The solid line is the seasonal SD of Niño-3 averaged over all the 30-yr base periods during 1871–2000. (b) The seasonal SD of Niño-3 as functions of the 30-yr base periods and seasons. (c) The seasonal SD of Niño-3 averaged in the NDJ (solid line) and MAM (dashed line) seasons. In (a) and (b) the months on the *x* axis are at the centers of the seasons. In (b) and (c) the years on the *y* axis are at the centers of the 30-yr base periods. In (b) the contour interval is 0.1°C, and values less than 0.7° and greater than 1° are shaded.

suspect that the interannual signal is weak in PDO and NAO and that the SD is sensitive to noise in the data.

An issue related to the interdecadal changes of ENSO variance is the interdecadal changes of ENSO predictability. One way of measuring predictability is to calculate the seasonal *P*. Here the seasonal *P* is measured by the autocorrelation of seasonal anomalies at a two-season lag. The seasonal *P* averaged over eleven 30-yr base periods shows that the seasonal *P* is usually large in the eastern equatorial Pacific and the related regions: the tropical Atlantic and tropical Indian Ocean (Fig. 10). The seasonal *P* is also seasonally dependent. For example, in the eastern equatorial Pacific, the seasonal *P* is largest in summer and smallest in winter. In the tropical Atlantic, the seasonal *P* is largest in spring and smallest in summer. The seasonal *P* in the Indian Ocean varies both regionally and seasonally. There is some persistence ($P > 0.4$) in the eastern Indian Ocean in winter and spring and some in the western Indian Ocean in autumn.

The interdecadal changes of the seasonal *P* of Niño-3 are shown in Fig. 11. It is seen that the seasonal *P* is largest (0.75) in summer and smallest (0.1) in winter. This is related to the so-called spring barrier of persistence. The persistence barrier is a result of the phase locking of ENSO to the annual cycle, which tends to cause transitions in ENSO indices to occur during boreal spring (Torrence and Webster 1998). In models, a similar spring barrier of predictability is attributed to the low ENSO variance during spring (Xue et al. 1994). The *P* in winter (averaged *P* for DJF) varies from -0.1 to 0.4 and has a sharp dip around 1965. In contrast, the *P* in

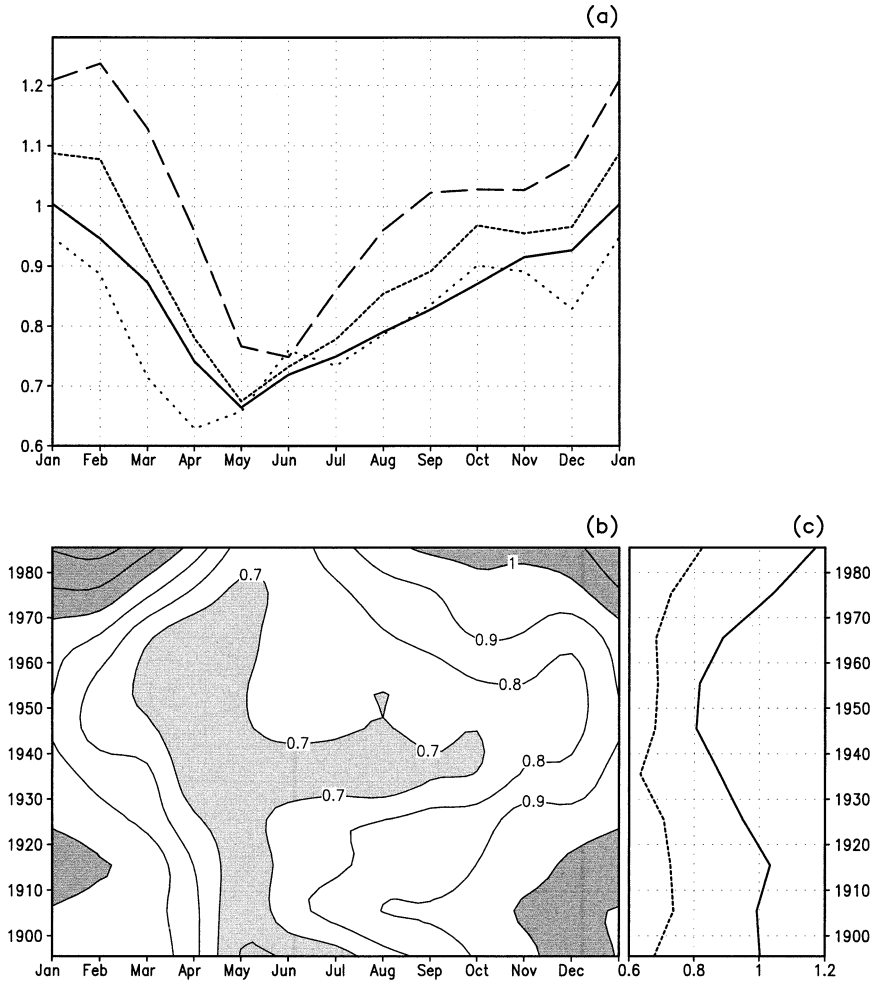

FIG. 9. Same as Fig. 8 but for the seasonal SD of the Darwin sea level pressure (hPa).

summer (averaged P for JJA) varies from 0.7 to 0.8. The seasonality of P, measured by the differences of P in summer and winter, varies interdecadally: weak during 1885–1910, moderate during 1920–50, strong during 1955–75, and moderate since 1975. The interdecadal changes of the seasonal P have an important implication for ENSO forecasting. If $P = 0.4$ is regarded as the lower limit of predictability, the heavy solid line ($P > 0.4$) in Fig. 11b marks the seasons from which ENSO is predictable up to a 6-month lead. During the predictable seasons, the predictability is high during 1885–1920, low during 1920–40, and high during 1950–2000. Note that the interdecadal changes of the seasonal P and its seasonality discussed above are also found in HadISST.

We have also studied the interdecadal changes of the seasonal P of the North Atlantic (NATL) and SATL. For SATL, the average seasonal P over eleven 30-yr base periods has a weak seasonality: largest (0.5) in spring and smallest (0.3) in summer. The interdecadal changes of the seasonal P of SATL in the past 130 yr have an amplitude of 0.1–0.2, which is largely consistent between ERSST and HadISST (not shown). For NATL, the seasonal P is about 0.4–0.5 and has some interdecadal changes that are not consistent between ERSST and HadISST. We conclude that the interdecadal variability of the seasonal P for NATL is not resolved well by the datasets.

5. Conclusions and discussion

The recently developed long interpolated historical SST datasets (ERSST and HadISST) by Smith and Reynolds (2003) and RAY, respectively, gave us a unique opportunity to address the interdecadal changes of 30-yr SST normals in the past 130 yr. A 30-yr SST normal includes both climatological mean and standard deviation. The seasonal CM has the largest interdecadal variations (0.3°–0.6°) in the tropical Indian Ocean, the midlatitude North Pacific, the midlatitude North Atlantic, most of the South Atlantic, and the sub-Antarctic front (Fig. 1). The seasonal SD is prominent in the eastern equatorial Pacific, the North Pacific, and the North Atlantic (Fig. 7). The seasonal SD in Niño-3 varies in-

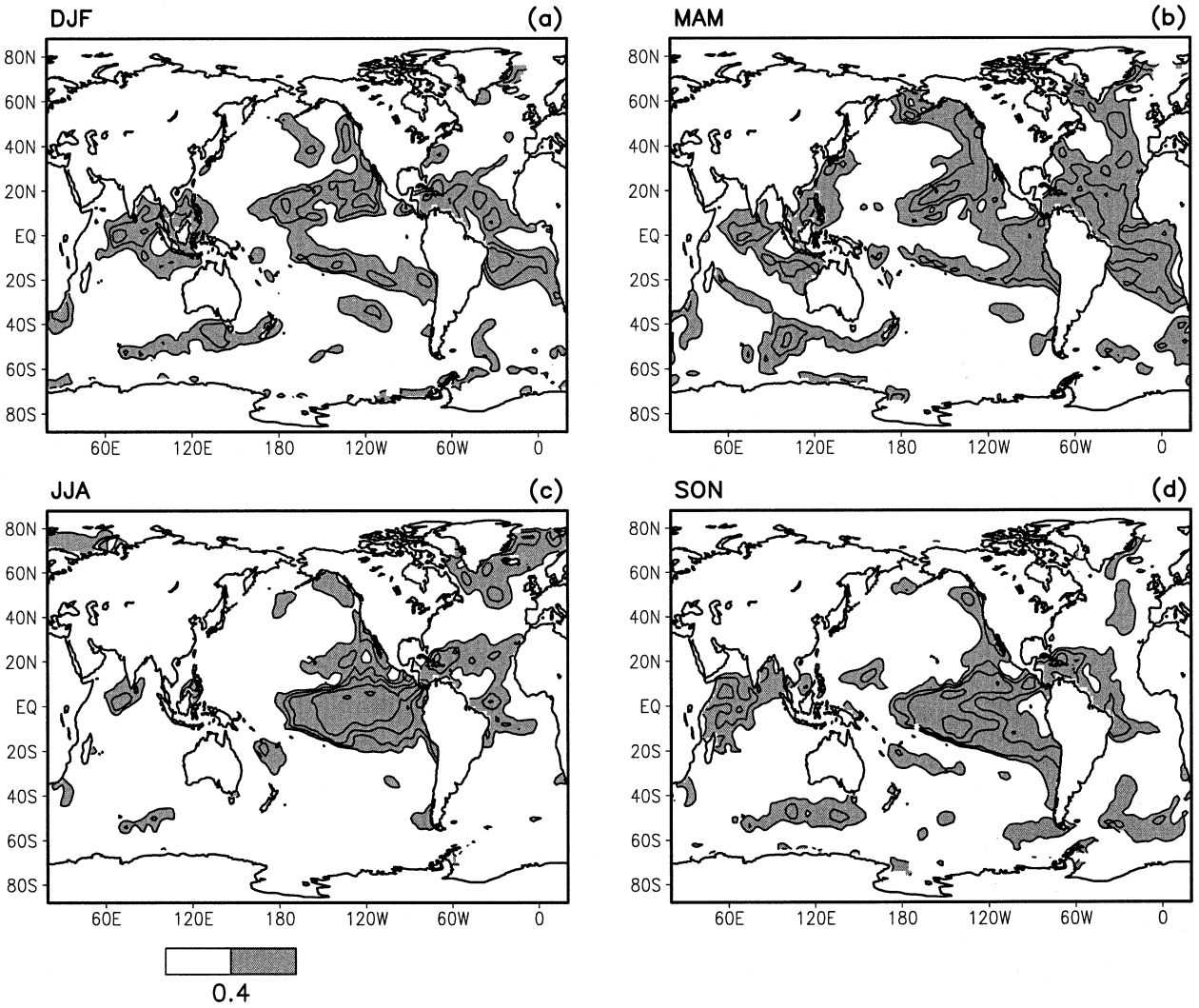

FIG. 10. The seasonal persistence of ERSST averaged over all the 30-yr base periods during 1871–2000 in the (a) DJF, (b) MAM, (c) JJA, and (d) SON seasons. The contour interval is 0.1. Contours less than 0.4 are omitted and values greater than 0.4 are shaded.

terdecadally: intermediate during 1885–1910, small during 1910–65, and large during 1965–2000, which is consistent with previous studies (Torrence and Compo 1998; Kestin et al. 1998).

We also studied the seasonal persistence, measured by the autocorrelation of seasonal anomalies at a two-season lag. The seasonal *P* of Niño-3 is largest (0.75) in summer and smallest (0.1) in winter (Fig. 11a). The seasonality of *P* in Niño-3 varies interdecadally: relatively weak during 1885–1910, moderate during 1910–55, strong during 1955–75, and moderate during 1975–2000 (Fig. 11b).

There are three kinds of explanation about the interdecadal changes of ENSO variability. One assumes that El Niño–Southern Oscillation is a natural mode, attributable to ocean–atmosphere interactions. Because this natural model is neutrally stable, random atmospheric disturbances contribute to its irregularities (Penland and Sardeshmukh 1995). Another explanation assumes that the ocean–atmosphere coupled system is highly nonlinear and is able to generate a chaotic behavior by itself (Tziperman et al. 1995). The third assumes that the properties of ENSO, period and intensity, change when the background climate state changes (Kirtman and Schopf 1998; Fedorov and Philander 2000). This explanation relates the change of ENSO properties to the low-frequency variability that modulates the background state in records for the past century. Whether the upward trend observed in the past few decades is related to global warming is another challenging question that remains to be answered (Trenberth 1998).

The interdecadal changes of SD and *P* have important implications for ENSO forecasting. For example, when the SD of Niño-3 is small, during 1910–65, the seasonal *P* is low, and so predictability is low; when the SD of Niño-3 is high, during 1881–1910 and 1965–2000, the

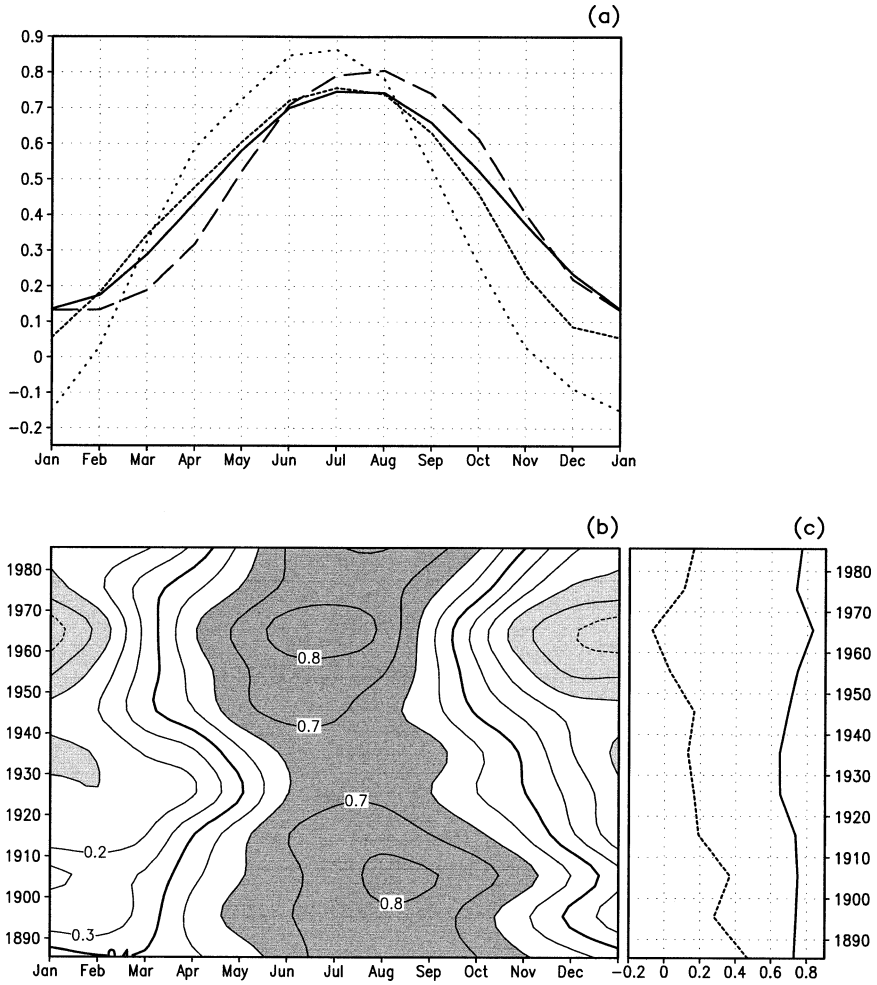

FIG. 11. (a) Annual cycle of the seasonal P of Niño-3 for the 1971–2000 (long dash), 1961–90 (short dash), and 1951–80 (dot) base periods. The solid line is the seasonal P of Niño-3 averaged over all the 30-yr base periods during 1871–2000. (b) The seasonal P of Niño-3 as functions of 30-yr base periods and seasons. (c) The seasonal P of Niño-3 averaged in the JJA seasons (solid line) and the seasonal P of Niño-3 averaged in the DJF seasons (dash line). In (a) and (b) the months on the x axis are at the centers of the seasons. In (b) and (c) the years on the y axis are at the centers of the 30-yr base periods. In (b) values less than 0.1 and greater than 0.6 are shaded, and the 0.4 contour is thickened.

seasonal P is high, and so predictability is high. The interdecadal changes of the seasonality of SD and P of Niño-3 are also important for ENSO forecasts. During 1955–75 when the spring barrier of persistency is high, all models show some degree of spring barrier in forecast skill. Since 1975, however, when the spring barrier of persistence became weaker than before, the spring barrier of model forecast skill is reduced (Balmaseda et al. 1995). Because the SD and P of Niño-3 change significantly from one 30-yr base period to another, it is important to update them periodically. For example, during the last three 30-yr base periods (1951–80, 1961–90, and 1971–2000), the SD of Niño-3 increased about 17% in spring over consecutive base periods (Fig. 8a). Thus, the SD should be updated to prevent amplitude errors in standardized anomaly forecasts of Niño-3.

Periodically updating the 30-yr normals is also important in monitoring and diagnosing both high- and low-frequency variability. The study shows that in the Indian Ocean low-frequency variability is largely a linear trend upon which interannual variability has some seasonal persistence ($P > 0.4$; Figs. 2 and 10). In the North Pacific, low-frequency variability has a multidecadal oscillation upon which interannual variability has little seasonal persistence (Figs. 3 and 10). In the North Atlantic, low-frequency variability has a multidecadal oscillation that has a shorter timescale than that of the North Pacific, and interannual variability has little seasonal persistence (Figs. 4 and 10). In the tropical Atlantic, low-frequency variability is prominent in the south tropical Atlantic only, but high-frequency variability is prominent in both the south and north tropical

Atlantic and has some seasonal persistence ($P > 0.4$; Figs. 1 and 10). We found that the datasets are not accurate enough to address the interdecadal changes of the high-frequency variability in any of the ocean basins except those in the eastern equatorial Pacific. Because we use two well-known SST analyses in the study, the results on the high- and low-frequency SST variability over the global ocean are probably reliable and can serve as references for future research on similar topics.

Acknowledgments. We thank the two anonymous reviewers for comments and suggestions, which helped us to improve the manuscript significantly. We also thank Vernon Kousky, Arun Kumar, and Huug van den Dool of the Climate Prediction Center for providing useful comments on the manuscript.

REFERENCES

Allan, R. J., 2000: ENSO and climatic variability in the past 150 years. *El Niño and the Southern Oscillation Multiscale Variability and Its Impacts on Natural Ecosystems and Society,* H. F. Diaz and V. Markgraf, Eds., Cambridge University Press, 1–55.

——, N. Nicholls, P. D. Jones, and I. J. Butterworth, 1991: A further extension of the Tahiti–Darwin SOI, early events and Darwin pressure. *J. Climate,* **4,** 743–749.

Balmaseda, M. A., M. K. Davey, and D. L. T. Anderson, 1995: Decadal and seasonal dependence of ENSO prediction skill. *J. Climate,* **8,** 2705–2715.

Bottomley, M., C. K. Folland, J. Hsiung, R. E. Newell, and D. E. Parker, 1990: *Global Ocean Surface Temperature Atlas ''GOSTA.''* HMSO, London, 20 pp+iv, 313 plates.

Enfield, D. B., and A. M. Mestas-Nuñez, 2000: Global modes of ENSO and non-ENSO SST variability and their associations with climate. *El Niño and the Southern Oscillation Multiscale Variability and Its Impacts on Natural Ecosystems and Society,* H. F. Diaz and V. Markgraf, Eds., Cambridge University Press, 89–112.

Fedorov, A. V., and S. G. Philander, 2000: Is El Niño changing? *Science,* **288,** 1997–2002.

Folland, C. K., D. E. Parker, A. Colman, and R. Washington, 1999: Large scale modes of ocean surface temperature since the late nineteenth century. *Beyond El Niño: Decadal and Interdecadal Climate Variability,* A. Navarra, Eds., Springer-Verlag, 73–102.

Houghton, J. T., Y. Ding, D. J. Griggs, M. Noguer, P. J. van der Linden, X. Dai, K. Maskell, and C. A. Johnson, Eds., 2001: *Climate Change 2001: The Scientific Basis.* Cambridge University Press, 881 pp.

Kaplan, A., M. A. Cane, Y. Kushnir, A. C. Clement, M. B. Blumenthal, and B. Rajagopalan, 1998: Analysis of global sea surface temperature 1856–1991. *J. Geophys. Res.,* **103,** 18 567–18 589.

Kestin, T. S., D. J. Karoly, J.-I. Yano, and N. A. Rayner, 1998: Time–frequency variability of ENSO and stochastic simulations. *J. Climate,* **11,** 2258–2272.

Kirtman, B. P., and P. S. Schopf, 1998: Decadal variability in ENSO predictability and prediction. *J. Climate,* **11,** 2804–2822.

Klein, S. A., B. J. Soden, and N.-C. Lau, 1999: Remote sea surface temperature variations during ENSO: Evidence for a tropical atmospheric bridge. *J. Climate,* **12,** 917–932.

Kushnir, Y., 1994: Interdecadal variations in North Atlantic sea surface temperature and associated atmospheric conditions. *J. Climate,* **7,** 141–157.

Mantua, N. J., S. R. Hare, Y. Zhang, J. M. Wallace, and R. C. Francis, 1997: A Pacific interdecadal climate oscillation with impacts on salmon production. *Bull. Amer. Meteor. Soc.,* **78,** 1069–1079.

Mestas-Nuñez, A. M., and D. B. Enfield, 2001: Eastern equatorial Pacific SST variability: ENSO and non-ENSO components and their climatic associations. *J. Climate,* **14,** 391–402.

North, G. R., T. L. Bell, and R. F. Cahalan, 1982: Sampling errors in the estimation of empirical orthogonal functions. *Mon. Wea. Rev.,* **110,** 699–706.

Penland, C., and P. D. Sardeshmukh, 1995: The optimal growth of tropical sea surface temperature anomalies. *J. Climate,* **8,** 1999–2024.

Power, S., T. Casey, C. Folland, A. Colman, and V. Mehta, 1999: Inter-decadal modulation of the impact of ENSO on Australia. *Climate Dyn.,* **15,** 319–324.

Rayner, N. A., D. E. Parker, E. B. Horton, C. K. Folland, L. V. Alexander, and D. P. Rowell, 2003: Global analyses of SST, sea ice, and night marine air temperature since the late nineteenth century. *J. Geophys. Res.,* in press.

Reynolds, R. W., and T. M. Smith, 1995: A high-resolution global sea surface temperature climatology. *J. Climate,* **8,** 1571–1583.

——, N. A. Rayner, T. M. Smith, D. C. Stokes, and W. Wang, 2002: An improved in situ and satellite SST analysis for climate. *J. Climate,* **15,** 1609–1625.

Smith, T. M., 2000: Tropical Pacific sea level variations (1948–98). *J. Climate,* **13,** 2757–2769.

——, and R. W. Reynolds, 1998: A high-resolution global sea surface temperature climatology for the 1961–90 base period. *J. Climate,* **11,** 3320–3323.

——, and ——, 2003: Extended reconstruction of global sea surface temperatures based on COADS data (1854–1997). *J. Climate,* **16,** 1495–1510.

——, ——, R. E. Livezey, and D. C. Stokes, 1996: Reconstruction of historical sea surface temperatures using empirical orthogonal functions. *J. Climate,* **9,** 1403–1420.

Torrence, C., and G. P. Compo, 1998: A practical guide to wavelet analysis. *Bull. Amer. Meteor. Soc.,* **79,** 61–78.

——, and P. J. Webster, 1998: The annual cycle of persistence in the El Niño–Southern Oscillation. *Quart. J. Roy. Meteor. Soc.,* **124,** 1985–2004.

Trenberth, K. E., 1998: El Niño and global warming. *J. Mar. Educ.,* **15,** 12–18.

Tziperman, E., M. A. Cane, and S. Zebiak, 1995: Irregularity and locking to the seasonal cycle in an ENSO prediction model as explained by the quasi-periodicity route to chaos. *J. Atmos. Sci.,* **52,** 293–306.

Xue, Y., M. A. Cane, S. E. Zebiak, and B. Blumenthal, 1994: On the prediction of ENSO: A study with a low-order Markov model. *Tellus,* **46A,** 512–528.

Zhang, Y., J. M. Wallace, and D. S. Battisti, 1997: ENSO-like interdecadal variability: 1900–93. *J. Climate,* **10,** 1004–1020.